Motion of the cello bridge

Ailin Zhang[a)]
College of Mathematics and Statistics, Shenzhen University, 3688 Nanhai Avenue Shenzhen, Guangdong, People's Republic of China

Jim Woodhouse
Department of Engineering, University of Cambridge, Trumpington Street, Cambridge CB2 1PZ, United Kingdom

George Stoppani
6 Needham Avenue, Chorlton-cum-Hardy, Manchester M21 8AA, United Kingdom

(Received 24 May 2016; revised 12 September 2016; accepted 22 September 2016; published online 14 October 2016)

This paper presents an experimental investigation of the motion of the bridge of a cello, in the frequency range up to 2 kHz. Vibration measurements were carried out on three different cellos, and the results used to determine the position of the Instantaneous Centre of rotation of the bridge, treated as a rigid body. The assumption of rigid body rotation is shown to give a good approximation up to at least 1 kHz. The instantaneous centre moves from the sound-post side of the bridge at the lowest frequencies towards the bass-bar side at higher frequencies, remaining close to the surface of the top plate of the instrument. The trajectory as a function of frequency sheds light on the response of the cello in response to excitation by bowing the different strings. The correlation between the motion at the four string notches and directly measured transfer functions at these four notches is examined and verified for some important low-frequency body resonances.
 [http://dx.doi.org/10.1121/1.4964609]

[JW] Pages: 2636–2645

I. INTRODUCTION

The bridge on most bowed string instruments is made from specially selected maple. It is held in place only by the tension of strings, and plays a critical transfer role between the vibrating strings and the radiating corpus during sound production on the instrument. An intelligently cut and well fitted bridge can have a profound influence on the tonal characteristics of a bowed string instrument, as makers and players have been aware for centuries.

The bridge has also attracted interest from scientists. Research up to 1993 has been summarized by Hutchins and Benade.[1] Minnaert and Vlam[2] reported the first detailed investigation into the flexural, torsional, and transverse vibration of a violin bridge using a specially designed optical system. The first study on the motion of a cello bridge was done by Bladier[3] in 1960 using a piezoelectric transducer fastened to the tested bridge. He showed differences between the motions at the two bridge feet. In 1979, Reinicke[4] displayed the motion of a violin bridge and a cello bridge using hologram interferometry, and modelled the motions mathematically. Experiments on the design of the violin bridge were made by Müller[5] in 1979. He measured the sound pressure with differently designed bridges and discussed the function of the bridge. Cremer[6] described this work in his remarkable book summarizing knowledge about the violin family up to 1983.

Rodgers and Masino[7] and Kishi and Osanai[8] examined bridge motion under different conditions using finite element analysis. On a more practical level, Jansson and his co-workers[9–11] investigated the effect of bridge modification on the vibrational behaviour of the instrument. They started with the influence of wood removal from different areas of the bridge and then turned their attention to the bridge foot spacing. Trott[12] used a shaker and an impedance head to measure the power input to a violin bridge when excited in various positions and directions.

The first work that relates directly to the present study came from Marshall,[13] who observed that a violin bridge shows more motion at the bass foot than at the treble foot up to 700 Hz. Later modal and acoustical measurements exploring the action of the violin bridge as a filter were carried out by Bissinger.[14] His experimental results also showed a transition of the predominant motion of the feet of a violin bridge from the bass side to the treble side, confirming and extending the findings of Marshall.

This observation links to a familiar claim about the role of the soundpost in violin-family instruments: the soundpost produces a constraint near the treble foot of the bridge at low frequencies, inducing asymmetry in the vibration patterns and boosting the sound radiation in the monopole-dominated regime at low frequencies (see, for example, Cremer[6]). The effect is sometimes informally described by saying that the bridge "rocks around the soundpost" at low frequencies. The transition documented by Marshall and Bissinger may define the correct sense of "at low frequencies." Some authors have taken to referring to this frequency range as the "transition region," and a feature commonly seen in violin

a)Electronic mail: az304@szu.edu.cn

 0001-4966/2016/140(4)/2636/10/$30.00

frequency response has been dubbed the "transition hill" (see, for example, Gough[15]). This phenomenon is the main topic of the present work. Detailed measurements of bridge motion will be shown, and analyzed in a way that gives a new perspective on this transition.

The measurements also shed light on another question of some current interest, relating to possible differences in coupling to the instrument body of the four separate strings. The single most common acoustical measurement on violin-family instruments is an approximation to the driving-point admittance (or mobility) at the top of the bridge. Most researchers use some version of a technique originated by Jansson,[16] in which a force is applied to one corner of a bridge, usually by a miniature impulse hammer, and the motion is measured at the other corner using a laser vibrometer or miniature accelerometer. For a detailed discussion of such measurements and their interpretation, see Woodhouse and Langley.[17] It would be very useful to quantify how well this corner-to-corner measurement in fact represents the admittance felt by the four individual strings at their respective bridge notches, in the usual bowing direction tangential to the bridge top. For a perfect match to all four strings, the motion of the top part of the bridge would need to follow around the line of the curved shape of the bridge.

Another way to pose this requirement, familiar to mechanical engineers (see, for example, Meriam *et al.*[18]), is to say, that the "instantaneous center of rotation" of the top part of the bridge would need to lie at the geometric center of the bridge-top curve. This formulation stems from a theorem of kinematics: planar motion of any rigid body, at any given instant, can be represented completely by rotation at some angular velocity about a point known as the instantaneous center (IC). The suggestion that the bridge "rocks around the soundpost at low frequencies" is, of course, a direct claim about the position of the IC. In the context of small vibration governed by linear theory, it is natural to examine the motion associated with the separate harmonic frequencies making up the admittance function, and in those terms the IC can be expected to move around as a function of frequency. When its trajectory lies near the geometric center of the bridge curve, the four strings will "feel" the body response in a similar way, accurately represented by the standard measurement. If it lies far from that point, however, the strings will experience significantly different responses.

The work reported here will use this paradigm to examine the motion of a cello bridge in the low- to mid-frequency range, where its in-plane motion can be expected to be essentially rigid. The cello bridge, which is very different from a violin bridge in proportions, has been less emphasized in the musical acoustics literature. As well as having intrinsic interest, its larger size makes the necessary measurements easier. Vibration transfer function measurements at several points around the bridge and on the top plate near the bridge feet were carried out on three cellos. The responses at these points at any given frequency were processed to find the best-fitted rigid-body motion of the bridge, from which the IC can be located. This IC position can then be tracked as a function of frequency, giving an immediate visual test of how strong a constraint the soundpost offers, and an impression of how similar or different the body response will appear to the four strings.

It is perhaps worth stating explicitly what will *not* be covered here. Modal analysis of the bridge to show the deformations at higher frequencies has been well covered in previous work, and will not be repeated here. The first deformational resonance of the bridge will set the upper limit to the frequency range of interest here: around and above that frequency, "hill-like" features in the instrument response are to be expected, as has been discussed in various earlier literature (see, for example, Ref. 17). At lower frequencies, although there will be some discussion of resonances of the cello body in relation to wolf notes and other playability issues, detailed modal analysis of the body is not directly relevant to the agenda here. The clear and restricted aim of this study is to visualise the associated bridge motion in a novel way via the trajectory of the IC. This will have implications for the "transition region," and also for issues of playability such as the notorious cello wolf note.[19] Playability differences between the strings of the instrument will be discussed, and possible limitations of the conventional single measurement of bridge admittance.

II. EXPERIMENTS

A. Instruments to be tested

Systematic experiments were conducted on three different cellos, which were fitted with different shapes of bridges. For convenience, these three cellos are labelled Cello 1, Cello 2, and Cello 3 in the remainder of this paper. The first cello was a student instrument of moderate quality, made by an unknown maker, fitted with a Belgian design bridge. The upper body shape and longer legs of Belgian bridges are generally thought to give a brighter and louder sound. The width between the outside foot-edges is 90 mm, and the height from the middle point of its bass bar side foot to its top is 95 mm. The second cello is one made some forty years ago by the second author, fitted with a French design bridge. The length of legs of this bridge accounts for approximately half its height, shorter than those of the Belgian counterpart. The width between its outside foot-edges is 92 mm and the height from the middle point of its bass bar side foot to its top is 91 mm. In general, French bridges appear lower and wider than their Belgian counterparts, and are often said to be somewhat darker sounding. The third cello is a new instrument made by the third author. It has a typical Belgian design bridge, which shares the same outline dimensions as the first one.

B. Measurement procedure

To resemble the holding manner of a player, the cellos were held for testing within a steel support frame, steadied by soft foam pieces in a similar way to the player's knees. The cello endpin was located in a hole at the base of the rig, and the neck was fastened by a cable tie to a shaped and rubber-lined block behind the neck in first position. This rig is described in more detail in an earlier paper.[20] All

experiments reported here were carried out with the cello strings correctly tuned and thoroughly damped, and all took place in the same laboratory acoustic environment.

Figure 1 shows the positions of a set of test points on a cello bridge, and the directions of force application at these points in order to measure transfer functions. The C-string corner of the cello bridge is denoted as point 1. Points 1–5 are located on the edge of the cello bridge. Points 6 and 7 cannot be excited directly, but the results are deduced by averaging measurements made on the top plate near the feet, symmetrically placed in front and behind the two positions. Points 8–11 denote the positions of the string notches under the C, G, D, and A strings, respectively. The geometric center of the bridge-top curve is marked by a cross-in-circle symbol.

The motion was measured at the C string corner by a small accelerometer (DJB M2222C) glued to the bridge. It was orientated so that its center line was parallel to the usual bowing direction of the cello C string. The accelerometer mass (including some allowance for its cable) is around 0.8 g, compared with a typical mass of a cello bridge around 19 g. A miniature force hammer (PCB 086D80) held in a pendulum fixture was used to provide a reliably positioned force pulse to each point of interest on the cello bridge or top plate. The set of points shown in Fig. 1 were hit by the hammer in turn. All the hammer impacts were applied in the plane of the bridge or parallel to it. Forces labelled as F1 and F3 were applied to points 1 and 3 on the bridge along the bowing direction of the nearest strings. Impulses labelled as F2, F4, and F5 were applied to Points 2, 4, and 5 on the sides of the bridge perpendicular to the surface. Impact forces on the body to deduce points 6 and 7 were perpendicular to the top plate. The input and output signals, after buffering with suitable charge amplifiers, were processed by data logging software to yield the transfer functions associated with the seven points. These will be used for calculating the planar motion of the cello bridge in Sec. III: The measurements will be interpreted using the familiar reciprocal theorem of linear vibration, as if they were the *motion* at the test points in response to *force* applied at the bridge corner.

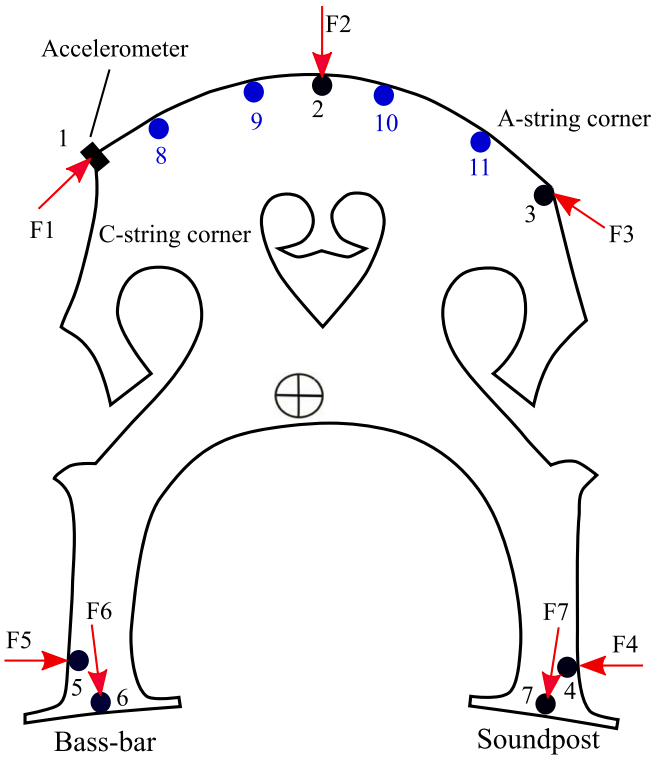

FIG. 1. (Color online) Positions and directions of applied forcing at points around a cello bridge (points 1–7), together with the positions of the four string notches (points 8–11). Cross-in-circle symbol: the geometric center of the bridge-top curve.

The bridge of cello 1, in addition to the accelerometer, was fitted with four piezoelectric force sensors to record the transverse force exerted by the vibrating strings, as described in earlier work.[20] These additional sensors, with their attached cables, add mass and damping to the bridge and thus modify the response somewhat, but were necessary to obtain the vibration response associated with excitation at the four separate string notches as described earlier[20] and discussed further in Sec. IV.

III. CALCULATION OF BRIDGE MOTION

In the lower frequency range, the bridge is expected to move approximately as a rigid body with little deformation. A simple least-squares calculation can be used to determine that rigid motion from the set of measurements described in Sec. II B. The position of the IC can then be deduced. To describe the bridge motion, first choose a reference point O and define Cartesian axes X, Y at this point as shown in Fig. 2. Any rigid motion of the bridge in this plane can now be described by a linear velocity at O with components (U, V), together with an angular velocity Ω about the axis through O perpendicular to the plane. At a particular measurement point on the bridge with position vector (x_j, y_j) relative to O, the velocity vector is then

$$\boldsymbol{u_j} = (U - \Omega y_j, V + \Omega x_j), \tag{1}$$

where $j = 1, 2, ..., 7$.

The measured velocity at the test points (obtained by integrating the accelerometer signal) will be the component of this velocity in a particular direction determined by the orientation of the hammer impact. Denoting the unit vector in that direction by

$$\boldsymbol{n_j} = (\cos\varphi_j, \sin\varphi_j), \tag{2}$$

the measured velocity associated with the rigid bridge motion would be

$$t_j = \boldsymbol{u_j} \cdot \boldsymbol{n_j} = (U - \Omega y_j)\cos\varphi_j + (V + \Omega x_j)\sin\varphi_j. \tag{3}$$

The task now is to best-fit a rigid bridge motion to the set of measurements, to determine U, V, and Ω. A natural approach is to seek to minimise the error measure

$$\rho = \sum_j |m_j - t_j|^2, \tag{4}$$

where the measured velocities are denoted m_j. A standard least-squares procedure leads to a set of linear equations for the three unknowns. The position of the IC can then easily

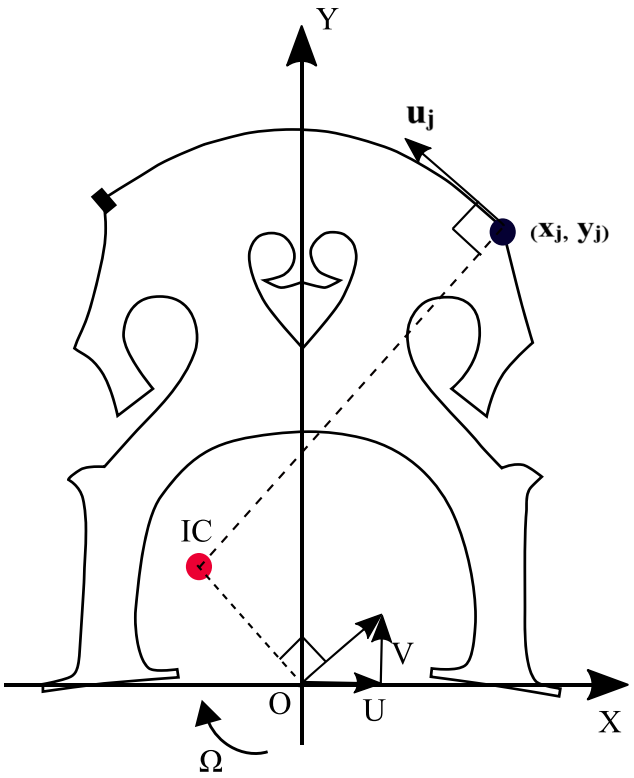

FIG. 2. (Color online) Schematic illustration of a cello bridge rotating rigidly about an instantaneous center.

be found. This point is defined by the fact that it has no linear velocity, so from Eq. (1) the coordinates of the IC relative to O are given by

$$X_{\rm ic} = -V/\Omega,$$
$$Y_{\rm ic} = U/\Omega. \tag{5}$$

However, there is a complicating factor to be considered. The measured values will be complex numbers, reflecting the fact that at any given frequency there may be a phase difference between the force and the velocity. In consequence the fitted U, V, and Ω will be complex, and the coordinates $X_{\rm ic}$ and $Y_{\rm ic}$ are thus also complex. To see what this means for the trajectory of the IC during a cycle of the vibration (known as the "centrode"[18]), it is convenient to write explicitly

$$U = U_0 \cos(\omega t + \xi_1),$$
$$V = V_0 \cos(\omega t + \xi_2),$$
$$\Omega = \Omega_0 \cos(\omega t + \xi_3). \tag{6}$$

Without loss of generality, define the instant $t = 0$ so that $\xi_3 = 0$. Then

$$X_{ic} = \frac{V_0 \cos(\omega t + \xi_2)}{\Omega_0 \cos \omega t} = -\frac{V_0}{\Omega_0}(\cos \xi_2 - \sin \xi_2 \tan \omega t),$$
$$Y_{ic} = \frac{U_0 \cos(\omega t + \xi_1)}{\Omega_0 \cos \omega t} = \frac{U_0}{\Omega_0}(\cos \xi_1 - \sin \xi_1 \tan \omega t). \tag{7}$$

The interpretation of these equations is that during one cycle of oscillation the IC moves along a straight line, with distance along this line parameterised by $\tan \omega t$. This motion involves travelling to infinity and then back from the opposite direction. This apparently rather drastic and non-physical behaviour has a simple interpretation: if the rotational component of motion is not in phase with the linear motion, there will be an instant when there is no rotation but non-zero linear velocity, and this requires the center of rotation to be "at infinity" at that instant. However, for the practical cases to be shown shortly it is invariably true that the vast majority of the time is spent near the point where the tangent function is zero, and discussions will focus on the position of that point: the movement "to infinity" can be ignored for the purposes of visualizing the main motion at the string notches.

IV. EXPERIMENTAL RESULTS

A. Bridge motion

A typical example of the trajectory of the IC is shown in Fig. 3, for the case of Cello 1 at an important frequency: 173 Hz, the "wolf note" frequency. The seven test points and four string notches are shown. A narrow elliptical patch around each point denotes the predicted displacement of that point, on an exaggerated scale. The line of circles marks the trajectory of the IC during one period. The predicted straight line is evident, with most points clustering beneath one bridge foot, near the top of the soundpost, which is the position on the straight line where the tangent function equals zero. This is the single position that will be plotted in the remainder of this article.

The motion shown in Fig. 3 is based on the least-squares fitting procedure described earlier. Figure 4 shows how well the measured motion at the seven points is approximated by the best-fitted rigid motion. Solid lines through each point

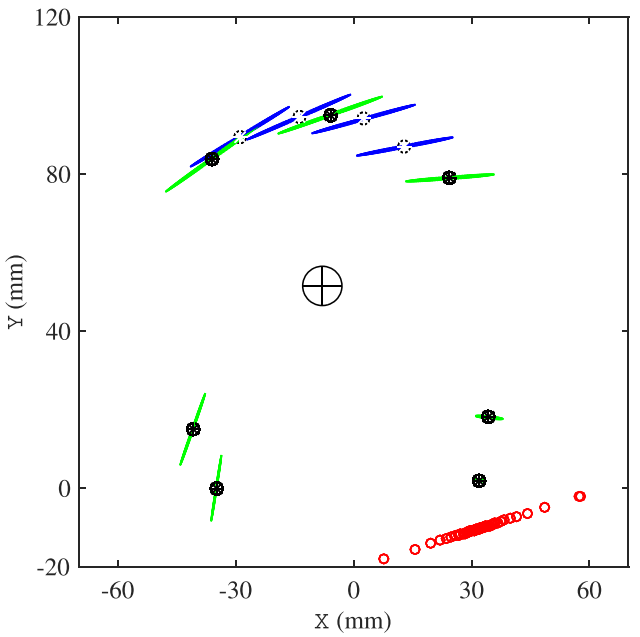

FIG. 3. (Color online) Predicted motion of the seven test points and four string notches from Fig. 1 for a resonance of cello 1 at frequency 173 Hz. The line of circles shows the trajectory of the IC during one period.

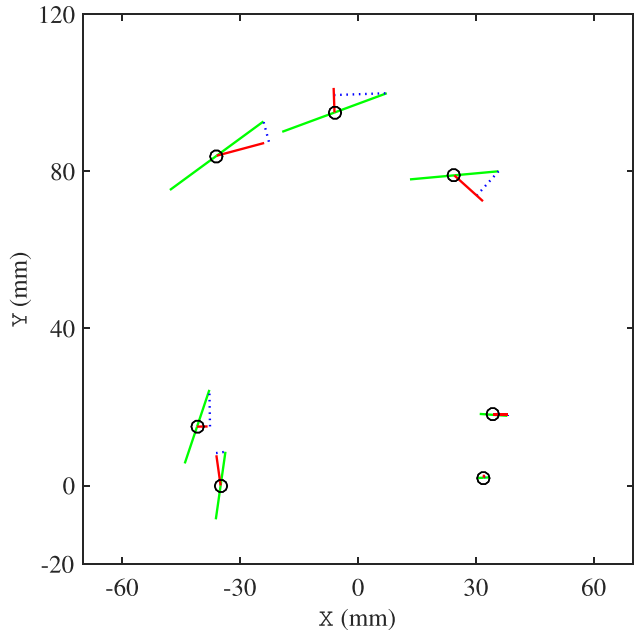

FIG. 4. (Color online) Predictions (double-ended solid lines) and measurements (single-ended solid lines) of the motions of the seven test points (circles) on the bridge of Cello 1 at 173 Hz. Dotted lines indicate the projections of predicted motions onto the measurement directions.

mark the major axis of the elliptical patches shown in Fig. 3, joining the two maximum values of predicted displacement at each point. Another solid line from each test point indicates the measured displacement of that point: These lines are, of course, confined to the component of motion aligned with the measurement direction in each case. Dotted lines indicate the projection of the predicted displacements along the measurement directions, which are in all cases close to the measured results. To judge the corresponding accuracy of fitting over the entire frequency range relevant to the discussion in this paper, Fig. 5 shows a plot of the normalised error

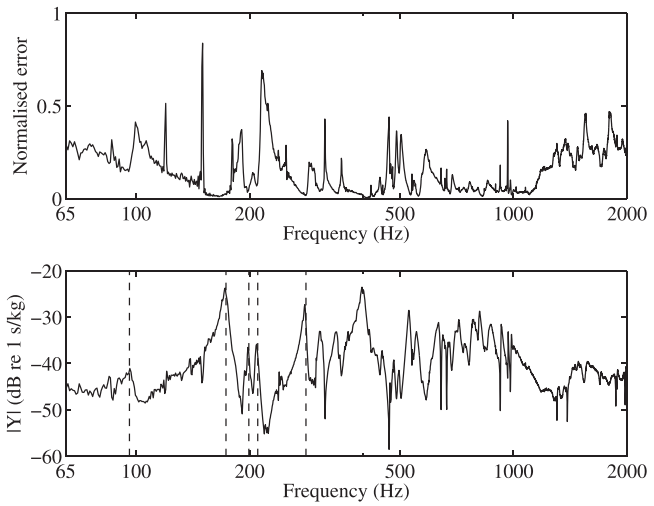

FIG. 5. Normalized error of fitted rigid-body motion of the bridge of Cello 1 (upper panel, see text for details); and its input admittance (lower panel). Vertical dashed lines in the lower panel mark resonances studied in detail later.

$$\rho_{\text{norm}} = \frac{\sum_j |m_j - t_j|^2}{\sum_j |m_j|^2}. \tag{8}$$

Figure 5 also shows, in the lower panel, the mobility transfer function for this cello at point F3, which is the usual approximation to the input admittance for all four strings, used frequently in earlier literature.[16] The comparison of the two panels reveals that the accuracy of fitting of rigid-body motion is generally good, i.e., the value of the error is low, whenever the response is high, i.e., near the modes of the cello body. At very low frequencies the fit is rather less accurate, mainly because the measurement noise is higher since the measured accelerations are small. There are occasional spikes of high error, but these correspond either to frequencies of electrical interference or to frequencies where the motion is small so the signal-to-noise ratio in the measurements is poor.

The lower panel of Fig. 5 also indicates, as vertical dashed lines, a few individual resonance frequencies of the cello. One of these, at 173 Hz, is the frequency studied in Figs. 3 and 4; it is what used to be called the "main body resonance" of the cello, responsible for the notorious "wolf note." More will be said about this particular resonance in Sec. V. The other highlighted resonances will be examined later, in Figs. 8 and 10.

The behaviour of the IC is illustrated in two different forms in Figs. 6 and 7. Figure 6 shows the spatial trajectory of the IC. The seven test points and the four string notches are shown for spatial orientation, and the track of the IC as frequency varies is indicated by the trail of circles. This figure is divided into four frequency ranges. It can be seen that the IC tends to move between the two bridge feet: it falls predominantly on the sound-post side in the frequency range from 65 to 205 Hz, then moves towards the bass-bar side in the frequency range from 205 to 466 Hz, clusters in the middle of the two feet over the frequency range from 466 to 1200 Hz, and finally moves somewhat back towards the sound-post side before 2000 Hz. Only in a rather narrow frequency range around 1300 Hz does the IC move upwards from near the top plate surface. It only pays rather rare visits to the vicinity of the geometric centre of the bridge curve.

The X and Y coordinates of the IC are plotted against frequency over the range 65–2000 Hz in Fig. 7, for all three of the cellos studied here. The dashed lines indicate the zero levels of each plot, for an origin of coordinates halfway between the soundpost and bass-bar feet. The vertical scales give values for Cello 1, while the results for Cellos 2 and 3 have been lifted by 100 and 200 mm, respectively, for clarity. The general pattern is very similar for all three cellos, and has also been shown to be robust in repeated tests on any given cello, not shown here. Re-measuring on a different day, with complete re-rigging of the apparatus, gave good repeatability—a mean deviation of the IC position across the entire frequency range of 6 mm in the X coordinate and 8 mm in the Y coordinate. This deviation is small compared to the movement of the IC revealed in the plots, so that the trends revealed here are robust.

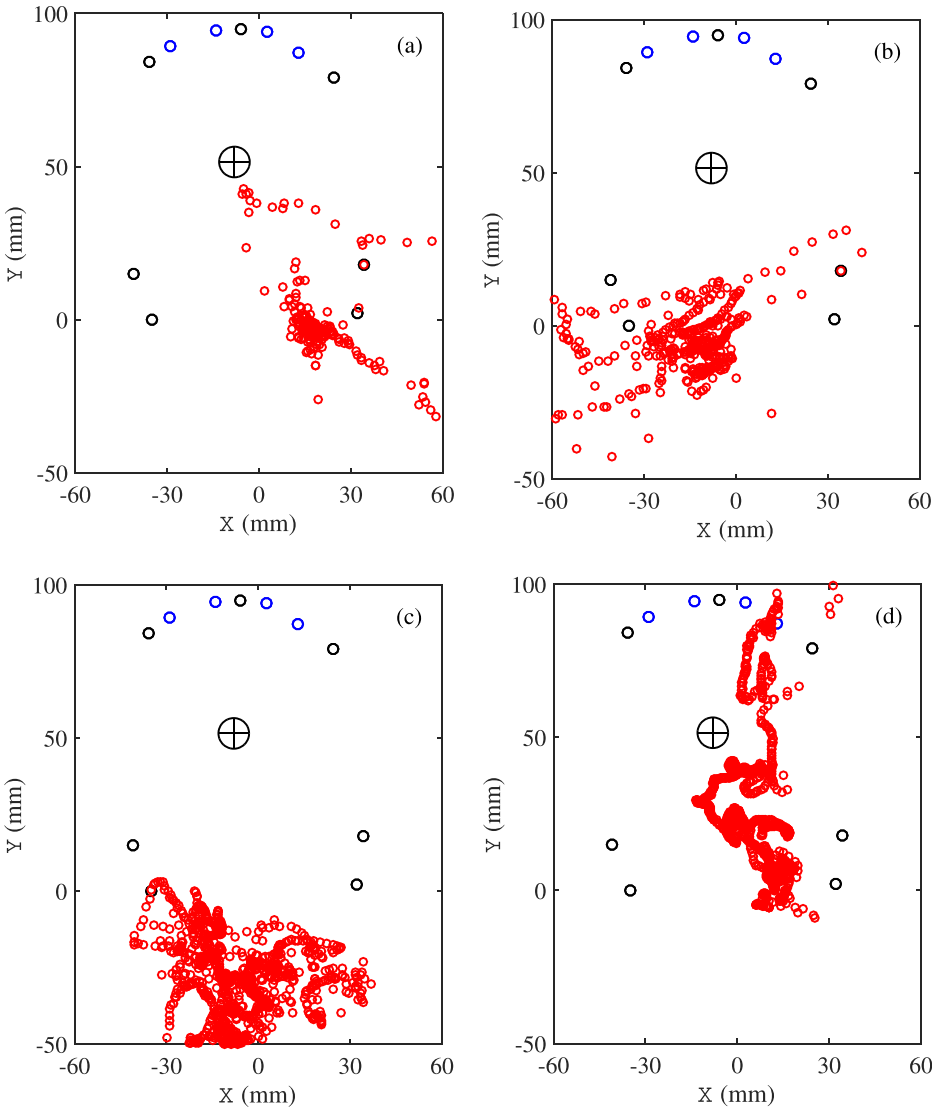

FIG. 6. (Color online) Trajectories of the IC of the bridge of Cello 1 over four frequency ranges: (a) 65–205 Hz; (b) 205–466 Hz; (c) 466–1200 Hz; (d) 1200–2000 Hz. Circles show the positions of the test points and string notches, cross-in-circle symbol shows the geometric center of the bridge-top curve.

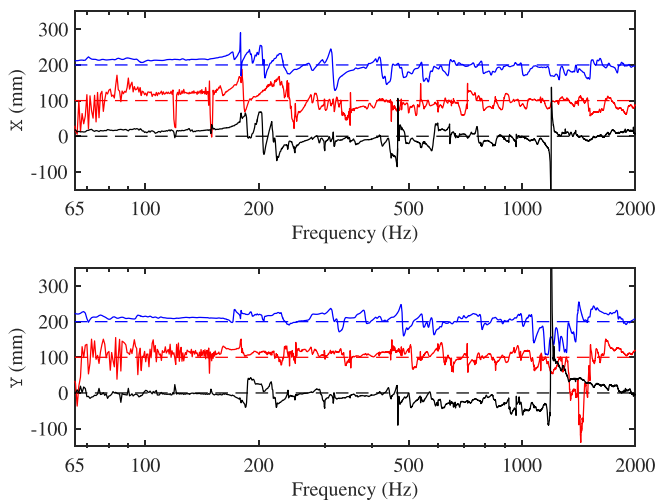

FIG. 7. (Color online) *X* and *Y* coordinates of the IC of the bridge of Cello 1 (lower line, data as in Fig. 6), Cello 2 (middle line), and Cello 3 (upper line) over the frequency range 65–2000 Hz. The data for Cello 3 has higher measurement noise at low frequencies. The plots are separated by 100 mm intervals for clarity.

Up to about 180 Hz, the IC stays close to the top of the soundpost. In the intermediate range from there up to about 700 Hz it tends to move back and forth between the bridge feet, always close to the surface of the cello top plate. The detailed movements are different for each cello because the well-separated resonances in this frequency range are different.

At higher frequencies still, the *X* position moves around in the vicinity of the mid-point between the bridge feet, but the *Y* position does something more interesting. For all three cellos a conspicuous feature appears in the range 1–1.5 kHz showing movement first down into the cello body and then jumping upwards before settling back towards the level of the bridge base. Digging further into the details of the measurements (not reproduced here), this feature turns out to be associated with the first resonance of the cello bridge: as shown by Reinicke[4] this involves lateral motion of the bridge top while the legs "sway" in shear. Reinicke shows this resonance occurring around 1 kHz for his particular cello bridge, with its feet rigidly clamped. The *in situ* bridge resonance for Cello 1 is found to occur at about 1200 Hz, and those for Cellos 2 and 3 at about 1500 and 1350 Hz, respectively. These frequencies match the visible features in the

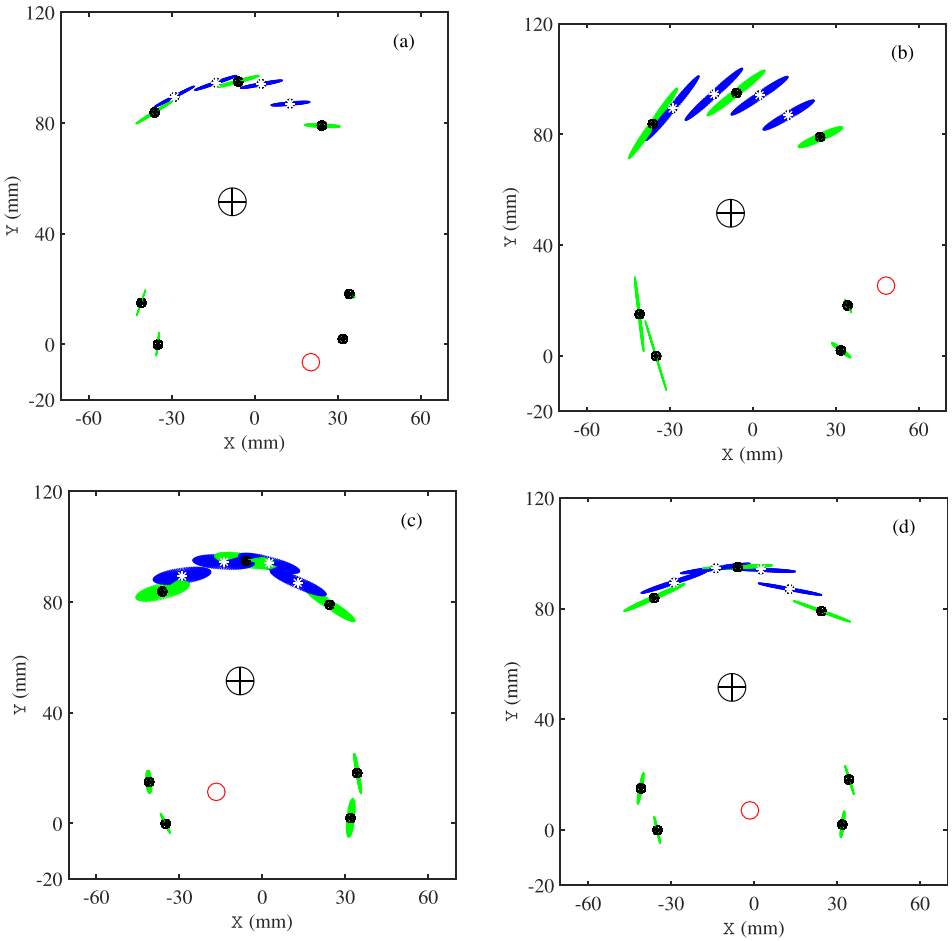

FIG. 8. (Color online) Predicted motion of the bridge of Cello 1 at four different resonances, in the same format as Fig. 3: (a) 97 Hz; (b) 200 Hz; (c) 209 Hz; and (d) 281 Hz.

fitted trajectories of the ICs shown in Figs. 6 and 7. Possibly the frequency is lower for cello 1 than for the others because of the extra mass of the force sensors built in to its bridge, as noted earlier. This bridge resonance sets a cutoff frequency beyond which the analysis and discussion in this paper is no longer appropriate.

B. Modal analysis of bridge vibrations

It is of particular interest to examine the motion of the cello bridge associated with resonance frequencies of the cello body. One such resonance has already been seen: The frequency chosen for Fig. 3 corresponds to a strong resonance of cello 1, the one responsible for its wolf note. Figure 8 shows a few more of the low resonances of this cello, at frequencies marked by the dashed lines in the lower plot of Fig. 5.

The first resonance, in Fig. 8(a), occurs at around 97 Hz and is the mode usually called A0: a modified Helmholtz resonance of the air cavity in the cello body.[6] The IC for the structural motion associated with this mode is close to the sound-post side foot, suggesting that the soundpost gives a hard constraint for this mode. The two small peaks near 200 Hz give bridge motions as shown in Fig. 8(b) and 8(c). Particularly in Fig. 8(c) the elliptical shape of the patches is more obvious than in the earlier plots, because the phase difference between translational and rotational motion is bigger. The final resonance illustrated corresponds to a prominent peak in the frequency response of Cello 1 at 281 Hz. The IC is now roughly halfway between the bridge feet, and the motions of the test points in Fig. 8(d) are thus rather symmetrical about the center line of the bridge.

V. BRIDGE MOTION AND THE RESPONSE OF SEPARATE STRINGS

As has been shown previously,[20] the transfer functions measured at the separate string notches on Cello 1 show some minor differences. These differences should relate directly to the motion of the cello bridge: The differences between the movements of the four string notches are responsible for the variations between the frequency response functions of the cello body felt by the separate strings. These variations in turn are likely to contribute to differences of playability between the strings on an instrument, as commonly reported by players.

The particular transfer functions available to make a comparison were measured by applying force at each string notch separately, along the corresponding bowing direction, and then measuring the resulting body response with the fixed accelerometer as in the measurements described in Sec. IV. Examples of these transfer functions are plotted in Fig. 9, over a low-frequency range that encompasses four clear resonances. In this case, force was applied by the breaking of a fine copper wire. This allows good control over the position and direction of the force, but does not give especially high signal-to-noise ratio, so the measurements

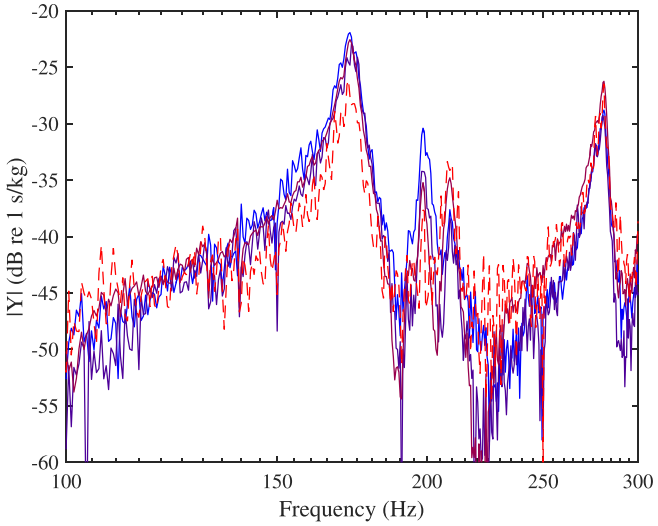

FIG. 9. (Color online) Measured transfer functions of cello 1 at the four string notches, with force input in the corresponding bowing directions, from 100 to 300 Hz. The result for the A string notch is shown dashed, the other three follow in a systematic order (see main text).

are more noisy than the more familiar hammer measurements, such as that shown in the lower plot of Fig. 5.

These transfer functions can be expressed in terms of the usual modal superposition:

$$Y_j(\boldsymbol{x_j}, \boldsymbol{x}', \omega) = i\omega \sum_n \frac{u_n(\boldsymbol{x_j}) u_n(\boldsymbol{x}')}{\omega_n^2 + 2i\omega\omega_n\zeta_n - \omega^2}, \tag{9}$$

where $j = 1, 2, 3, 4$ describes the four separate string notches, and mode n has natural frequency ω_n, damping factor ζ_n and mass-normalised mode shape $u_n(x)$. The position of the accelerometer at the C-string corner of the bridge is denoted by $\boldsymbol{x}'$, and the position of the relevant string notch by $\boldsymbol{x_j}$. It is immediately clear that the amplitude of mode n in this expression is proportional to the amplitude of the mode shape at the position of string notch j, in the corresponding bowing direction: all other factors are common to all four string notches. That means that the pattern of modal amplitudes should relate directly to the bridge motion at the four notches, discussed in earlier sections. These modal amplitudes can be determined from measured transfer functions by standard techniques of modal analysis (e.g., Ewins[21]): in this case circle-fitting has been used to determine amplitudes for the four modes apparent in Fig. 9.

These four resonances have already been studied, and the corresponding bridge motions shown in Figs. 3 and 8(b)–8(d). The movements of the four string notches along corresponding bowing directions at each of the four resonances are illustrated in Figs. 10(a)–10(d). These motions are compared with the deduced modal amplitudes in a similar

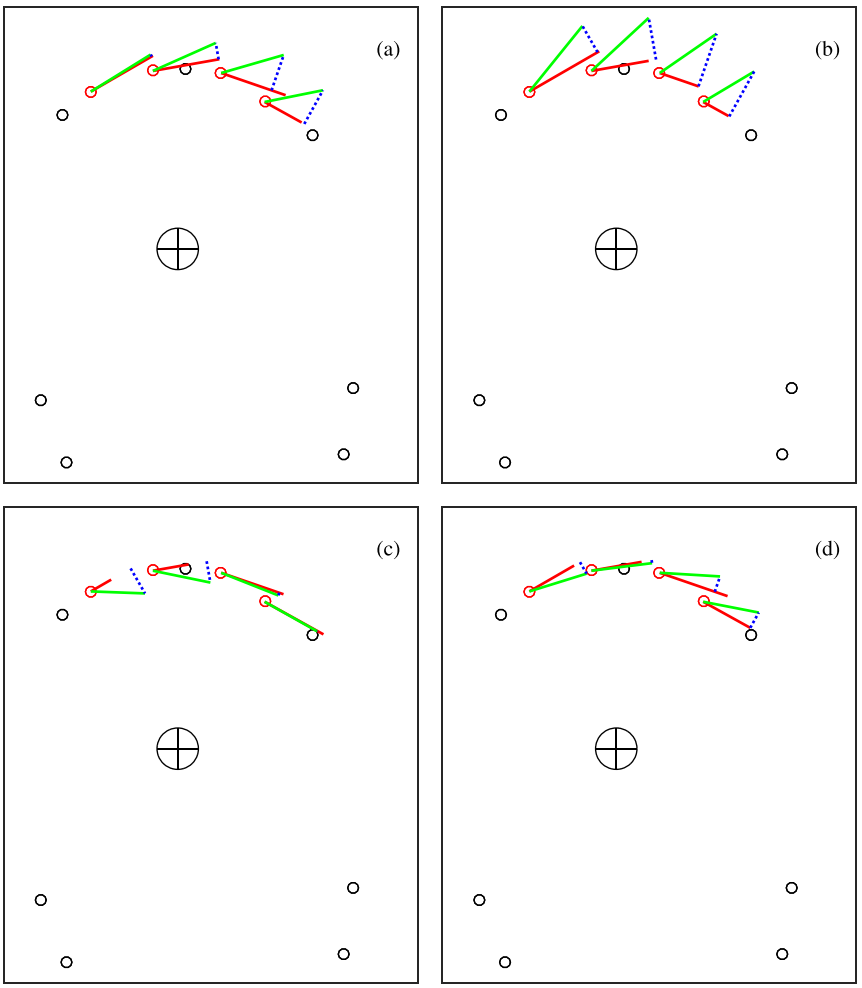

FIG. 10. (Color online) Movement of the four string notches of Cello 1 at four different resonances: (a) 173 Hz; (b) 200 Hz; (c) 209 Hz; and (d) 281 Hz. Motion in the bowing direction for each string determined by fitting to the measurements of Fig. 9 is shown, together with the predicted rigid-body motion and dotted projection lines to allow comparison.

format to Fig. 4. The test points and string notches are indicated by circles as before. For each mode in turn, solid lines indicate the measured modal amplitude in the bowing direction for each string and the maximum values of the predicted displacements as in Figs. 3 and 8; dashed lines show the projection of the predicted displacements in the bowing directions.

The comparison is encouragingly close, although by no means perfect because of experimental limitations. For the mode at 173 Hz, shown in Fig. 10(a), the predicted amplitude is highest at the C notch, and decreases progressively across the other three notches. The circle-fit amplitudes follow this pattern, except that the amplitude at the D notch is rather too high, perhaps a consequence of the limitation of fitting the noisy data of Fig. 9. The second resonance, at 199 Hz, shows a similar pattern of decreasing amplitudes from C to A notches, but more strongly than in the previous case. This pattern is directly apparent to the eye in the variation of peak heights in supplemental Fig. 11 (Ref. 22), and the results in Fig. 10(b) show a close match.

The third mode, at 209 Hz, shows the reverse pattern of amplitude variation because the IC has shifted to the bass-bar side. The measurements of Fig. 9 show this reversed pattern directly. Figure 10(c) shows good qualitative agreement, but the lower two strings do not agree in detail. It looks as if the IC was even further to left when the measurements of the four separate strings were made: Such a change is quite possible, because the two sets of measurements were separated by several months and the behaviour of the cello body may have changed a little in the interim because of factors like humidity variation. Finally the fourth mode, at 281 Hz, is predicted to have rather similar amplitudes at all four string notches because the IC is near the center-line of the bridge in this case. This prediction is well supported by the measurements.

VI. DISCUSSION AND CONCLUSIONS

The motion of the bridge on a cello in the low-frequency range has been studied in some detail. The observed bridge motion shows the characteristics of a rigid body for frequencies below the first deformational resonance of the bridge, which occurs in the range 1–1.5 kHz. By measuring the response to excitation at a number of points around the bridge and using a least-squares procedure to find the best-fitting rigid body motion, the trajectory of the IC has been mapped as a function of frequency. It tends to lie close to the bridge foot near the soundpost at the lowest frequencies, up to about 200 Hz, while at higher frequencies the IC moves towards the bass-bar foot and is most commonly found to lie near the mid-point between the two bridge feet. A broadly similar pattern has emerged from measurements on three different cellos.

These results give a very direct and intuitive confirmation of the qualitative notion that the soundpost provides a strong constraint at the lowest frequencies, and that the bridge does indeed "rock around the soundpost" for some important low modes responsible for considerable monopole sound radiation. In the cello a transition occurs near 200 Hz, above which the IC moves around in the vicinity of the mid-point between the bridge feet. This suggests that the motion of the two bridge feet will be broadly comparable above the transition, rather than the bass-bar side becoming dominant as has been suggested for the violin.[14]

The position of the IC gives an immediate way to visualise the balance across the four strings. For frequencies where the IC lies to the soundpost side of the center line, the bass strings will tend to be favoured. Conversely when it lies on the bassbar side, the treble strings will be favoured. But the commonest position throughout the frequency range 200–1000 Hz, where this analysis is appropriate, is close to the center line but well below the geometric center of the bridge-top curve. The result of such a placement will be a subtle favouring of the two middle strings relative to the outer strings. These effects are relatively small, but in musical acoustics it is never wise to disregard small effects: musicians can sometimes be very sensitive to them, a familiar example being the importance universally attached to small movements of a soundpost.

One application of the analysis of bridge motion is to study the interaction of the various strings with individual modes of the body. Examples have been shown to illustrate this, for four low-frequency modes of a particular cello. These examples demonstrate that a mode may be driven at similar magnitude by all strings, or there may be a significant increasing or decreasing trend from C string to A string in the strength of excitation by normal bowing of the string, all depending on the position of the IC. Players often comment on playability differences between the strings of an instrument, and this mechanism will contribute to those differences. For the particular case of the mode responsible for the "wolf note," at 173 Hz in this particular cello, the IC lies near the soundpost foot of the bridge, maximising the severity of the wolf on the lower strings (which are in any case more susceptible because of their higher impedance).

ACKNOWLEDGMENTS

This work was supported by National Natural Science Foundation of China (NSFC) Grant No. 11504246.

[1]C. M. Hutchins and V. Benade, *Research Papers in Violin Acoustics: 1975–1993, Section D* (Acoustical Society of America, New York, 1996).
[2]M. Minnaert and C. C. Vlam, "The vibrations of the violin bridge," Physica **4**(5), 361–372 (1937).
[3]B. Bladier, "On the bridge of the violoncello," Compt. Rend. **250**, 2161–2163 (1960).
[4]W. Reinicke, "Übertragungseigenschaften des streichinstrumentensteges" ("Transmission characteristics of stringed-instrument bridges"), J. Catgut. Acoust. Soc. **NL19**, 26–34 (1973).
[5]H. A. Müller, "The function of the violin bridge," J. Catgut. Acoust. Soc. **NL31**, 19–22 (1979).
[6]L. Cremer, *The Physics of the Violinm* (MIT Press, Cambridge, MA, 1984), Chaps. 9 and 13.
[7]O. E. Rodgers and T. R. Masino, "The effect of wood removal on bridge frequencies," J. Catgut. Acoust. Soc. **1**(6), 6–10 (1990).
[8]K. Kishi and T. Osanai, "Vibration analysis of the cello bridge using the finite element method," J. Acoust. Soc. Jpn. **47**(4), 274–281 (1991).
[9]E. V. Jansson, L. Fryden, and G. Mattsson, "On tuning of the violin bridge," J. Catgut. Acoust. Soc. **1**(6), 11–15 (1990).
[10]E. V. Jansson, "Experiments with the violin String and bridge," Appl. Acoust. **30**(2), 133–146 (1990).
[11]E. V. Jansson, "Violin frequency response—bridge mobility and bridge feet distance," Appl. Acoust. **65**(12), 1197–1205 (2004).
[12]W. J. Trott, "The violin and its bridge," J. Acoust. Soc. Am. **81**(6), 1948–1954 (1987).

[13]K. D. Marshall, "Modal analysis of a violin," J. Acoust. Soc. Am. **77**(2), 695–709 (1985).
[14]G. Bissinger, "The violin bridge as filter," J. Acoust. Soc. Am. **120**(1), 482–491 (2006).
[15]C. E. Gough, "Violin acoustics," Acoust. Today **12**(2), 22–30 (2016).
[16]E. V. Jansson, "Admittance measurements of 25 high quality violins," Acta Acoust. Acust. **83**, 337–341 (1997).
[17]J. Woodhouse and R. S. Langley, "Interpreting the input admittance of violins and guitars," Acta Acoust. Acust. **98**, 611–628 (2012).
[18]J. L. Meriam, L. G. Kraige, and J. N. Bolton, *Engineering Mechanics: Dynamics*, 8th ed. (Wiley, New York, 2016), Chap. 5.
[19]J. Woodhouse, "On the playability of violins: Part 2 Minimum bow force and transients," Acustica **78**, 137–153 (1993).
[20]A. Zhang and J. Woodhouse, "Reliability of the input admittance of bowed-string instruments measured by the hammer method," J. Acoust. Soc. Am. **136**, 3371–3381 (2014).
[21]D. J. Ewins, *Modal Testing: Theory, Practice, and Application* (Research Studies Press, Letchworth, UK, 1986), pp. 140–141.
[22]See supplemental Fig. 11 at http://dx.doi.org/10.1121/1.4964609.